Self-assembled single-crystal ferromagnetic iron nanowires formed by decomposition

Mohaddes-Ardabili, L.; Zheng, H.; Ogale, S. B.; Hannoyer, B.; Tian, W.; Wang, J.; Lofland, S. E.; Shinde, S. R.; Zhao, T.; Jia, Y.; Salamanca-Riba, L.; Schlom, D. G.; Wuttig, M.; Ramesh, R.

2004

Mohaddes-Ardabili, L., Zheng, H., Ogale, S. B., Hannoyer, B., Tian, W., Wang, J., et al. (2004). Self-assembled single-crystal ferromagnetic iron nanowires formed by decomposition. Nature Materials, 3, 533-538.

Self-assembled single-crystal ferromagnetic iron nanowires formed by decomposition

L. MOHADDES-ARDABILI[1], H. ZHENG[1], S. B. OGALE[1,2], B. HANNOYER[3],W.TIAN[4], J.WANG[1], S. E. LOFLAND[5], S. R. SHINDE[2],T. ZHAO[1],Y. JIA[4], L. SALAMANCA-RIBA[1], D. G. SCHLOM[4], M.WUTTIG[1] AND R. RAMESH[1,6,7*]

[1]*Department of Materials Science and Engineering, University of Maryland, College Park, Maryland 20742, USA*
[2] *Center for Superconductivity Research, Department of Physics, University of Maryland, College Park, Maryland 20742,USA*
[3] *Institut des Matériaux- LASTSM, Université de Rouen, BP 12, 76801 SER, France*
[4]*Department of Materials Science and Engineering, Pennsylvania State University, University Park, Pennsylvania 16802, USA*
[5]*Department of Physics, Rowan University, Glassboro, New Jersey 08028, USA*
[6]*Department of Materials Science and Engineering, University of California, Berkeley, California 94720, USA*
[7]*Department of Physics, University of California, Berkeley, California 94720, USA*
*e-mail: rramesh@uclink.berkeley.edu

Arrays of perpendicular ferromagnetic nanowires have recently attracted considerable interest for their potential use in many areas of advanced nanotechnology. We report a simple approach to create self-assembled nanowires of α-Fe through the decomposition of a suitably chosen perovskite. We illustrate the principle behind this approach using the reaction $2La_{0.5}Sr_{0.5}FeO_3 \rightarrow LaSrFeO_4 + Fe + O_2$ that occurs during the deposition of $La_{0.5}Sr_{0.5}FeO_3$ under reducing conditions. This leads to the spontaneous formation of an array of single-crystalline α-Fe nanowires embedded in $LaSrFeO_4$ matrix, which grow perpendicular to the substrate and span the entire film thickness. The diameter and spacing of the nanowires are controlled directly by deposition temperature. The nanowires show uniaxial anisotropy normal to the film plane and magnetization close to that of bulk α-Fe. The high magnetization and sizable coercivity of the nanowires make them desirable for high-density data storage and other magnetic-device applications.

Periodic arrays of perpendicular ferromagnetic nanowires have attracted significant attention owing to their prospective application in a variety of nanotechnological devices, especially in high-density recording media. An ideal recording medium in this regard consists of a densely organized assembly of nanometre-scale ferromagnets with high magnetization and suitable coercivity[1]. The formation of such a structure could either be process-directed or self-enabled. Although the former is more definitive and controlled, the latter is more desirable and convenient from the standpoint of ease of implementation, scaling up and cost-effectiveness. There are many examples of process-directed perpendicular nanowires[2], including those in which porous aluminium oxide films are used as a template and ferromagnetic metals such as Fe, Co and Ni

are electrodeposited into the pores of the film[3–7].However,much less effort has been put into the self-assembly of perpendicular ferromagnetic nanowires.

We report a simple scheme to create α-Fe nanowires by spontaneous phase decomposition of a suitably chosen parent compound, $La_{1-x}Sr_xFeO_3$ perovskite, during thin-film growth under specific conditions. $La_{1-x}Sr_xFeO_3$ belongs to the family of mixed-valent transition metal oxide perovskites[8]. The magnetic properties of such mixed-valent transition compounds are controlled by the superexchange mechanism between the $3d$ orbitals of the transition metal ions and the p orbitals of the oxygen ions[9]. Therefore, oxygen plays an important role in magnetic ordering of these compounds.

A single-phase $La_{0.5}Sr_{0.5}FeO_3$ target was used to grow thin films on single-crystalline $SrTiO_3$ (001) substrates by pulsed laser deposition (PLD).The films were deposited and cooled in vacuum (5 $\times10^{-6}$torr) at various temperatures ranging from 560 to 840 ℃ (see Supplementary Information for details of growth and characterization).The growth of epitaxial films of multicomponent perovskites such as $La_{0.5}Sr_{0.5}FeO_3$ by PLD is typically carried out under a relatively high oxygen background pressure of 100–200 mtorr in order to obtain a single-phase film[10]. Growth in 200 mtorr of O_2 at a substrate temperature of 760 ℃ yields single-phase epitaxial films with the perovskite structure (see Supplementary Information, Fig. S1, blue curve). X-ray diffraction (XRD) of the films grown in a vacuum environment (5 x 10^{-6} torr, obtained on a Siemens D5000 four-circle diffractometer), however, displays peaks that cannot be assigned to $La_{0.5}Sr_{0.5}FeO_3$ (Fig. S1; green curve). Figure 1a shows a low-magnification plan-view transmission electron microscope (TEM) image from a sample deposited at 760 ℃ under vacuum. The image clearly demonstrates that $La_{0.5}Sr_{0.5}FeO_3$has spontaneously decomposed into a fairly uniformly distributed second phase embedded in a matrix. The corresponding electron diffraction pattern from the sample (Fig. 1b) displays the epitaxial relationship between the matrix and the second phase and also indicates that only two phases exist. A low-magnification [001] dark-field TEM cross-section image (along the [100] zone axis) of the film is shown in Fig.1c. It reveals that the second phase shown in Fig. 1a comprises nanowires with an average diameter of 20 nm for the film grown at 760 ℃. Analysis of the XRD peaks and electron diffraction patterns yields the lattice parameters of the two phases as: nanowires $a=b=c=0.2864$ nm and matrix $a=b=0.3873$ nm, $c = 1.2776$ nm (± 0.0005 nm for all parameters).These lattice parameters are assigned to α-Fe with a body-centred-cubic (b.c.c.) structure ($a=0.287$ nm), based on the analysis below, and $LaSrFeO_4$ ($a=b=0.388$ nm, and $c=1.276$ nm; K_2NiF_4 structure).The latter is a known antiferromagnetic material with a Néel temperature of 380 K (ref.11).

Figure 2a shows a (001) high-resolution TEM cross-section image of a single nanowire embedded in the matrix. Figure 2b is an enlargement of the region marked by the rectangle in Fig. 2a. These images, together with the diffraction pattern shown in the inset of Fig. 2b,bring out the single-crystal character of a typical nanowire all along its length and the epitaxy between the matrix and nanowire both out-of-plane as well as in-plane.

The in-plane epitaxial relation of the two phases is obtained from plan-view electron diffraction (Fig. 1b): $[110]_{\alpha-Fe}||[100]_{LaSrFeO_4}$ and $[100]_{\alpha-Fe}||[110]_{LaSrFeO_4}$. The lattice parameter of b.c.c. iron ($a=0.2867$ nm) and spinel Fe_3O_4 ($a=0.8397$nm) are such that the lattice spacings are $d_{Fe\,110} \approx d_{Fe_3O_4\,400}$ and $d_{Fe\,200} \approx d_{Fe_3O_4\,440}$. Therefore, based on XRD and

electron diffraction patterns, it is also possible to interpret the second phase as Fe_3O_4. However, nanoprobe energy-dispersive X-ray spectroscopy (EDXS) analysis of the nanowires indicates that their main component is Fe with a small amount of oxygen, which could possibly arise due to beam spreading. EDXS analysis also confirmed the composition of the $LaSrFeO_4$ matrix, and reveals a La-to-Sr ratio close to 1, with a slight excess of La.

Conversion electron Mössbauer spectroscopy (CEMS) was used to identify the second phase precisely. Figure 3 shows the CEMS spectrum, recorded at room temperature, for the sample grown at 760 °C. The spectrum can be fitted with aquadrupole split doublet (area=47%) and a ferromagnetic sextet (area = 53%).The hyperfine parameters for the ferromagnetic sextet (isomer shift=0.00mms^{-1}, internal magnetic field= 32.9tesla) match perfectly with those of ferromagnetic α-Fe.

The paramagnetic doublet with quadrupole splitting of 1.40mms^{-1} and isomer shift of 0.36 mm s^{-1}is attributed to the matrix phase. A sextet in the Mössbauer spectrum is expected for antiferromagnetic $LaSrFeO_4$; however,the observation of a doublet indicates a paramagnetic state of the matrix.It has been shown that a slight change in *La:Sr* stoichiometry alters the magnetic and electronic properties of bulk $LaSrFeO_4$ (refs 12–14). In doped $La_{1-x}Sr_xFeO_4$, the Néel temperature decreases with xand the oxide is paramagnetic at room temperature.It is believed that doping disturbs the antiferromagnetic ordering of iron spins without any observable structural change. Similar behaviour is also observed in the $(La,Sr)_2CuO_4$ and $(La,Sr)_2NiO_4$ systems[15,16]. The asymmetry of the doublet and the degree of asymmetry relate to the specific angle between the electric field gradient and the gamma-ray beam, and is seen in most crystalline samples. The doublet is symmetric in powder samples, polycrystalline or multi-oriented domain systems. The epitaxy of the matrix phase in our case and the particular measurement geometry is the cause of the specific degree of asymmetry.

Taking into account the density and molecular weights of iron and $LaSrFeO_4$ (ref. 11), we can calculate the volume fraction of iron nanowires in the film from the areas of the Mössbauer spectral components. The calculation using 53% area represented by the magnetically split sextet shows that the iron nanowires comprise approximately 12% of the film volume. This value is in agreement with the estimated volume fraction obtained from the plan-view TEM image in Fig. 1a.Knowing the composition of the parent phase ($La_{0.5}Sr_{0.5}FeO_3$) and assigning the matrix and nanowire phases to $LaSrFeO_4$ and Fe, respectively,we can express the decomposition reaction as:

$$2La_{0.5}Sr_{0.5}FeO_3 \rightarrow LaSrFeO_4 + Fe + O_2 \tag{1}$$

Based on the crystal structure of the matrix and nanowires and using the above decomposition equation, the volume fraction of α-Fe in the film is calculated to be 10.95%, which is in fair agreement with the value calculated from both the Mössbauer spectroscopy and the TEM images. All the results suggest that the phase decomposition during deposition results in two essentially pure phases. This phase-decomposition route is different from reported epitaxial nanocomposites[17–22]; in our method a single-phase target is used and because of phase decomposition, the target phase is not one of the two phases present in the epitaxial nanocomposite.

Figure 4a compares the room-temperature magnetization data of the films grown in vacuum with those grown in 200 mtorr of oxygen at 760 ℃. Although no net magnetic moment exists in the film grown in oxygen (as expected for the antiferromagnetic $La_{0.5}Sr_{0.5}FeO_3$ perovskite phase),averystrong magnetic moment is observed forthe film grown in vacuum. The magnetization value normalized to the average α-Fe volume fraction obtained from Mössbauer spectra is about 1,600 e.m.u.cm^{-3}, which is fairly close to the magnetization of bulk iron (1,700 e.m.u.cm^{-3}). The 6% difference could possibly be attributed to surface spins and/or the error in the estimation of volume fraction used for normalization. In-plane and out-of-plane magnetic measurements reveal a strong out-of-plane magnetic anisotropy, with the easy axis along the long axis of the nanowires. A remanence of $M_r = 0.95\ M_s$ (where M_s is saturation magnetization) and coercivity of 3,400 Oe is observed for the films containing nanowires with diameter d=20 nm and length l=200 nm. An anisotropy field of ∼10,000 Oe is obtained from the magnetization measurements along the easy (out-of-plane) and the hard (in-plane) axes, as illustrated in Fig. 4a. Calculation of shape anisotropy[23] for a thin cylinder with an observed aspect ratio of (l/d) ≅ 10 using the measured value of M_s= 1,600 e.m.u.cm^{-3} yields an anisotropy field of H_{shape} = 9,535 Oe, which is in good agreement with the experimental value obtained. Figure 4b shows the dependence of the coercivity (obtained from out-of-plane hysteresis loops) on the aspect ratio for the wires with average diameter of 20 nm. A gradual increase of the coercivity is observed with increasing aspect ratio, but there is little change when l/d> 10.This is consistent with the result observed for iron nanowires, which were electrodeposited in porous alumite films[24].

Plan-view TEM images of the samples deposited at different temperatures reveal two interesting features of these nanostructures (see Supplementary Information, Fig. S2). As the growth temperature decreases, the diameter of the epitaxial nanowires decreases from 40–50 nm at 840 ℃ to 15–20 nm at 760 ℃ and finally to 4–6 nm at a deposition temperature of 560 ℃. The change in the diameter of the nanowires affects the characteristics of the corresponding hysteresis loop and makes it possible to tailor their magnetic properties. As an example, the variation of coercivity with respect to nanowire diameter (for a constant length) is shown in the inset to Fig. 4b. It follows a trend similar to that observed in electrodeposited iron nanowires[6]. The coercive field (H_c) exhibits a non-monotonic behaviour, initially increasing with the diameter up to a maximum value of ∼3,400 Oe at $d_{average}$ ≅20nm,dropping gradually with further increase in the diameter. A detailed analysis of the magnetic properties as a function of the nanowire diameter will be published separately.

Simultaneously, the cross-sectional shape of the nanowires changes with growth temperature. Plan-view high-resolution TEM images of individual nanowires in Fig. 5 show the changing cross-sectional shape and reveal low-index-faceted interfaces. The change in the lateral shape with decreasing temperature, from square (Fig. 5a) to octagonal cross-sections (Fig. 5b), and further to circular structures (Fig. 5c), can be explained as a consequence of the temperature dependence of the energy of the α-Fe/$LaSrFeO_4$ interface and the kinetics of its formation. At low deposition temperatures, diffusion is inhibited and the interface assumes the geometrically low-energy, circular shape. At higher temperatures, faceting will occur and the orientation of the facets will be determined by the crystallographic dependence of the interfacial energy. If the interfacial energy and its temperature dependence resemble that of the surface free-energy of iron, the observed temperature sequence of the faceting can be understood as a consequence of a

minimization of the surface energy of the Fe nanowires. For b.c.c. structures such as a-Fe, the closest-packed plane is (110).

The order of the surface free-energy for α-Fe (b.c.c.) is: $\gamma_{(110)} < \gamma_{(100)} < \gamma_{(111)}$ The $\gamma_{(110)}$ and $\gamma_{(100)}$ surface energies are very close to each other[25–27]. As the diameter of the nanowires increases, the differences in surface energy between the crystallographic planes of Fe become more significant. Thus, at intermediate growth temperatures, (110) and (100) facets become equivalent in dimension, giving rise to the octagonal cross-section of the nanowires. At higher temperatures, the (110) facets grow at the expense of the (100) facets, and square-shaped nanowires are formed. It is noteworthy that in all cases, the nanowires are single crystals and are hetero epitaxial with respect to the matrix as well as the substrate, clearly illustrating the dominant role of the substrate in controlling the number of variants of the α-Fe second phase.

The dimensions of the nanostructure are strongly temperature dependent. At higher deposition temperatures, α-Fe nanowires with larger lateral dimensions form. By reducing the temperature of deposition, the size and spacing between the iron nanowires decrease. This strong temperature dependence of the diameter of the nanowires, d, and their spacing, S, suggests a diffusion-controlled growth. The temperature dependencies of d and S can be approximately fitted to an Arrhenius-type plot yielding an activation energy of 1.2 eV for the reduction of $La_{0.5}Sr_{0.5}FeO_3$ and formation of the α-Fe nanowires. As the total volume of the decomposition products is constant at different temperatures of deposition, the fits conform to $d/S \approx$ constant. However, this ratio can be controlled through the amount of Fe that is available for the phase-decomposition reaction. For example, targets enriched with Fe yield a higher fraction of Fe nanowires.

The Arrhenius-type dependences of the dimensions of the epitaxial nanocomposite imply that the decomposition takes place at the deposition temperature, T_d. The reaction occurs at a very fine scale and creates interfaces of specific energy, γ. It will therefore take place at a temperature that is suppressed below the thermodynamic equilibrium temperature between the phases, T_e. The total interface energy can be approximated as $\alpha dh\gamma(\frac{L}{S})^2$. Here, the quantity α is a geometrical constant, and h and L^2 represent the nanowire height and the area of the film. This energy should correspond to the thermal energy $k(T_e - T_d)$. Because the ratio d/S is constant, it follows for constant geometry that $(T_e - T_d) \propto S^{-1}$. A logarithmic plot $\Delta T = (T_e - T_d)$ versus S should thus be approximately linear with a slope of –1. Figure 5d indicates that this is the case for $T_e \approx$ 1,140 K (ref.28).

Our approach to create self-assembled perpendicular arrays of single-crystal ferromagnetic Fe nanowires through the spontaneous phase-decomposition of a complex Fe oxide, can be expected to yield epitaxial nanocomposites from other complex oxides as well. Our preliminary studies have shown, for instance, that embedded cobalt nanowires can be grown by our process using a $La_{1-x}Sr_xCoO_3$ target. The remarkable feature of such nanostructures is the epitaxial orientation relationship between both phases and the substrate. More significantly, they exhibit a mutual heteroepitaxial relationship along the total length of the nanowire. Therefore, these nanostructures are illustrations of three-dimensional heteroepitaxy. The high magnetization, coupled with the controllable coercive field, makes these nanowire arrays desirable candidates for probe-based data-storage systems. Introducing long-range, two-dimensional translational

order over macroscopic distances among the nanowires will undoubtedly be a key enabler in this respect, and is an area that clearly warrants future exploration.

Competing financial interests

The authors declare that they have no competing financial interests.

References

1. Shiraki, M., Wakui,Y., Tokushima, T. & Tsuya, N. Perpendicular magnetic media by anodic oxidation method and their recording. *IEEE Trans. Magn*. **21**, 1465–1467 (1985).

2. Wagner, R. S. & Ellis, W. C. The vapor-liquid-solid mechanism of crystal growth and its application to silicon. *Trans. Metal. Soc. AIME* **233**, 1053–1064 (1965).

3. Li, F. & Metzger, R. M. Activation volume of α-Fe particles in alumite film. *J. Appl. Phys.* **81**, 3806–3808 (1997).

4. Huysmans, G. T. A., Lodder, J. C. & Wakui, J. Magnetization curling in perpendicular iron particle arrays (alumite media).*J. Appl. Phys*. **64**, 2016–2021 (1988).

5. Metzger, R. M. *et al*. Magnetic nanowires in hexagonally ordered pores of alumina. *IEEE Trans. Magn.* **36**, 30–35 (2000).

6. Sellmyer, D. J., Zheng, M. & Skomski, R. Magnetism of Fe, Co and Ni, nanowires in self-assembled arrays. *J. Phys. Condens. Matter* **13**, R433–R460 (2001).

7. Martń,J. I., Noguś, J.,Liu, K.,Vicente, J. L. & Schuller, I. K. Ordered magnetic nanostructures: fabrication and properties. *J. Magn. Magn. Mater*. **256**, 449–501 (2003).

8. Chainani, A., Mathew, M. & Sarma,D. D. Electronic structure of $La_{1-x}Sr_xFeO_3$. *Phys. Rev. B* **48**, 14818–14825 (1993).

9. Yang, J. B. *et al*. Crystal structure, magnetic properties, and Mössbauer studies of $La_{0.6}Sr_{0.4}FeO_{3-\delta}$ prepared by quenching in different atmospheres. Phys. Rev. B 66, 184415 (2002).

10. Chrisey, D. B & Hubler, G. K. (eds) *Pulsed Laser Deposition of Thin Films* (Wiley,New York, 1994).

11. Soubeyroux,J. L., Courbin, P., Fournes, P., Fruchart, D. & Le Flem, G. The phase $SrLaFeO_4$: magnetic and crystalline structure. *J. Solid State Chem*. **31**, 313–320 (1980).

12. Omata, T. *et al*. Electrical and magnetic properties of hole-doped $Sr_{1+x}La_{1-x}FeO_4$. *Phys. Rev. B* **49**, 10194–10199 (1994).

13. Omata, T. *et al*. Preparation of oxygen excess $SrLaFeO_{4+\delta}$and its electrical and magnetic properties. *Solid State Commun*.**88**, 807–811 (1993).

14. Omata, T. *et al*. Electronic structure of hole-doped $Sr_{1+x}La_{1-x}FeO_4$ studied by UPS and XAS. *Phys. Rev*. *B* **49**, 10200–10205 (1994).

15. Aharony, A., Birgeneau, R. J., Coniglio,A., Kastner, M. A. & Stanley, H. E. Magnetic phase diagram and magnetic pairing in doped La_2CuO_4. *Phys. Rev. Lett.* **60**, 1330–1333 (1998).

16. Cava, R. J. *et al*. Magnetic and electrical properties of $La_{2-x}Sr_xNiO_{4\pm\delta}$. *Phys. Rev. B* **43**, 1229–1232 (1991).

17. Nagao, M.,Tanaka,N. & Mihama, K. High resolution electron microscopy of composite films of gold and magnesium oxide. *Jpn J. Appl. Phys.* 25, L215–L218 (1986).

18. Catana,A., Broom, R. F.,Bednorz, J. G.,Mannhart, J. & Schlom,D. G. Identification of epitaxial Y_2O_3 inclusions in sputtered $YBa_2Cu_3O_7$ films: Impact on film growth. *Appl. Phys. Lett.* **60**, 1016–1018 (1992).

19. Lu, P. *et al*. High density, ultrafine precipitates in $YBa_2Cu_3O_{7-x}$ thin films prepared by plasma-enhanced metalorganic chemical vapor deposition. *Appl. Phys. Lett.* **60**, 1265–1267 (1992).

20.Atzmon, M., Kessler, D. A. & Srolovitz, D. J. Phase separation during film growth. *J. Appl. Phys.* 72, 442–446 (1992).

21. Moshnyaga,V. et al. Structural phase transition at the percolation threshold in epitaxial $(La_{0.7}Ca_{0.3}MnO_3)_{1-x}$: $(MgO)_x$ nanocomposite films. *Nature Mater.* 2, 247–252 (2003).

22. Zheng, H. *et al*. Multiferroic $BaTiO_3-CoFe_2O_4$ nanostructures. *Science* **303**, 661–663 (2004).

23. Bozorth, R. M. *Ferromagnetism* (IEEE Magnetics Soc., Piscataway, 1993).

24. Skomski,R.,Zeng, H. & Sellmyer, D. J. Magnetic localization in transition-metal nanowires. *Phys. Rev.B* **62**, 3900–3904 (2000).

25.Vitos, L., Ruban,A. V., Skriver, H. L. & Kollár, J. The surface energy of metals. *Surf. Sci.* **411**, 186–202 (1998).

26. Spencer, M. J. S., Hung,A., Snook,I. K. & Yarovsky, I. Density functional theory study of the relaxation and energy of iron surfaces. *Surf. Sci.* **513**, 389–398 (2002).

27.Aldén, M., Skriver, H. L.,Mirbt, S. & Johansson, B. Surface energy and magnetism of the 3d metals. *Surf. Sci.* **315**, 157–172 (1994).

28. Haasen, P. *Physical Metallurgy* 3rd edn (Cambridge Univ. Press, Cambridge, 1996).

List of Figures

Fig. 1   **TEM results of self-assembled nanostructures in $La_{0.5}Sr_{0.5}FeO_3$ thin films**.**a**,Plan-view TEM image from a film deposited in vacuum at T=760℃, showing the decomposition of the perovskite target into a second phase embedded in a matrix.**b**,Electron diffraction pattern illustrating the in-plane heteroepitaxy between $LaSrFeO_4$ and α-Fe. **c**,[001] dark-field cross-section image of a film showing α-Fe nanowires embedded in $LaSrFeO_4$matrix.

Fig. 2   **High-resolution cross-section images of a single α-Fe nanowire**. **a**, A single nanowire embedded in $LaSrFeO_4$ matrix. **b**, An enlargement of the region marked by the rectangle in **a**,which shows the single-crystalline nature of the nanowires.The inset shows the diffraction pattern of the area in **a** indicating the epitaxial relationship between α-Fe nanowires with the matrix.

Fig. 3   **Room-temperature [57]Co CEMS of the film deposited in vacuum**. Circles are experimental points and the black solid line is the fit. The spectrum is composed of a superposition of two sub-spectra: the sextet of ferromagnetic α-Fe (blue) and the paramagnetic doublet of the non-stoichiometric $LaSrFeO_4$ matrix (green).

Fig. 4   **Room-temperature magnetic properties of α-Fe nanowires. a**,Comparison of the magnetization of an antiferromagnetic $La_{0.5}Sr_{0.5}FeO_4$ epitaxial film grown in 200 mtorr O_2 (black) and of a film grown in vacuum at T= 760℃.Out-of-plane (blue) and in-plane (green) magnetic hysteresis loops correspond to α-Fe nanowires and indicate strong anisotropy. **b**,Coercivity versus aspect ratio (*l/d*)for the α-Fe nanowires with lateral dimension of *d* ≅20 nm.The inset shows the coercivity versus diameter for the samples grown at different temperatures.The error bars indicate 2% error,calculated by the standard deviation of the mean.

Fig. 5   **High-resolution plan-view TEM images of α-Fe nanowires showing the shape and lateral size dependence of the nanowires to deposition temperature**. **a**, Square-shaped 40–50 nm nanowires are obtained at T= 840 ℃. **b**, Octagonal cross section with d= 15–20 nm form at T= 760 ℃. **c**, Circular nanowires form at T= 560 ℃ (d= 4–6 nm). **d**, Logarithmic plot of normalized undercooling versus nanowire spacing for three different values of T_e. The slope of the straight line equals −1.
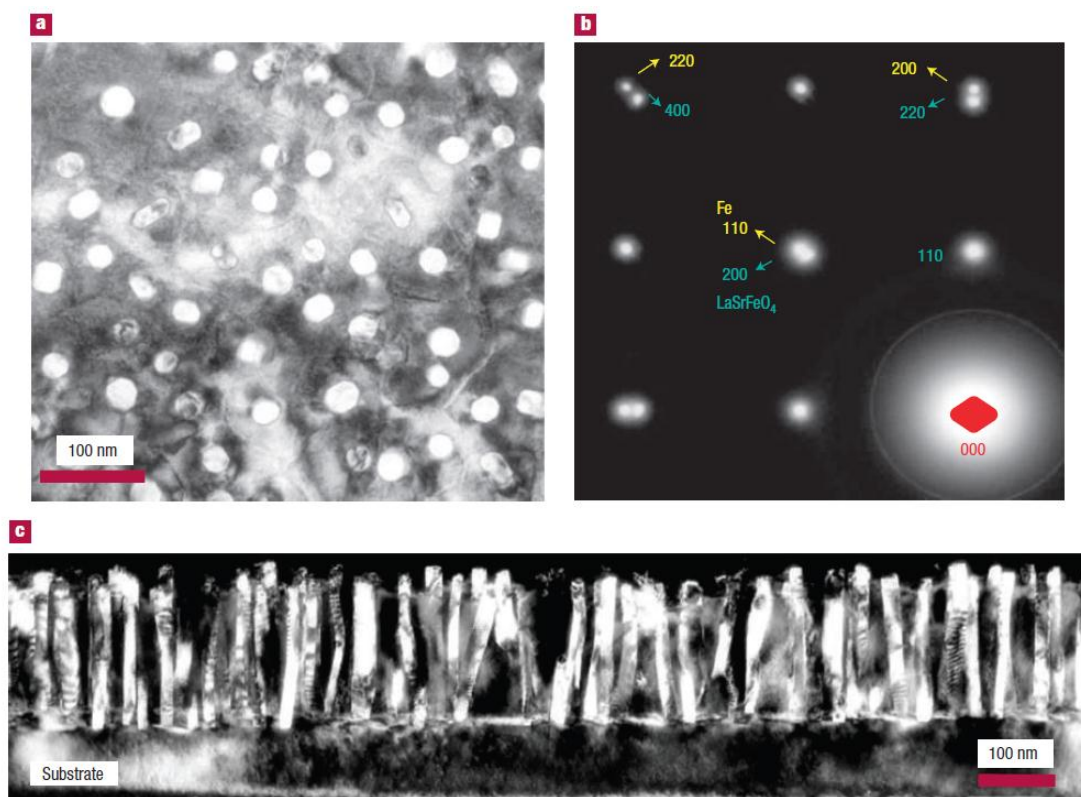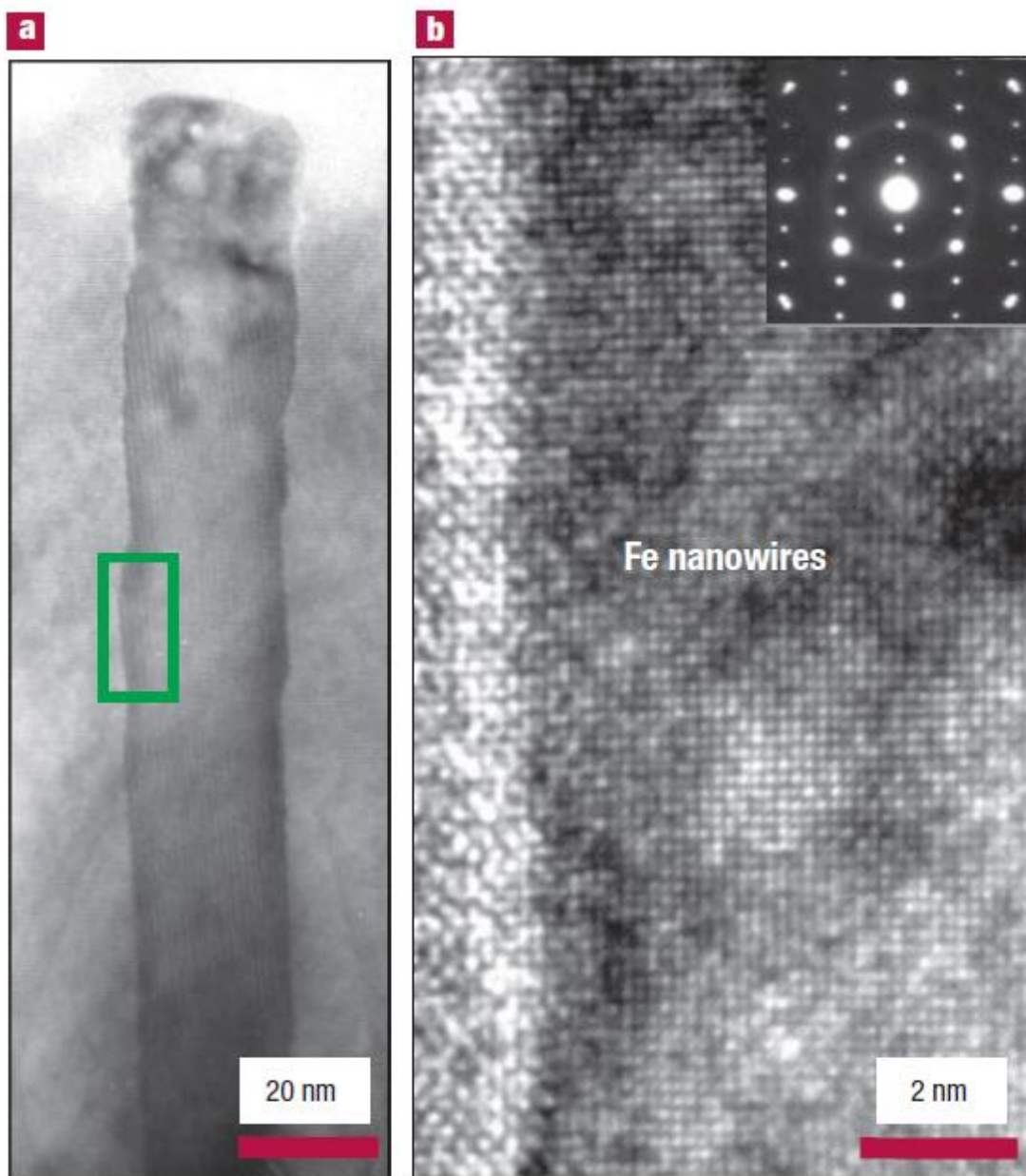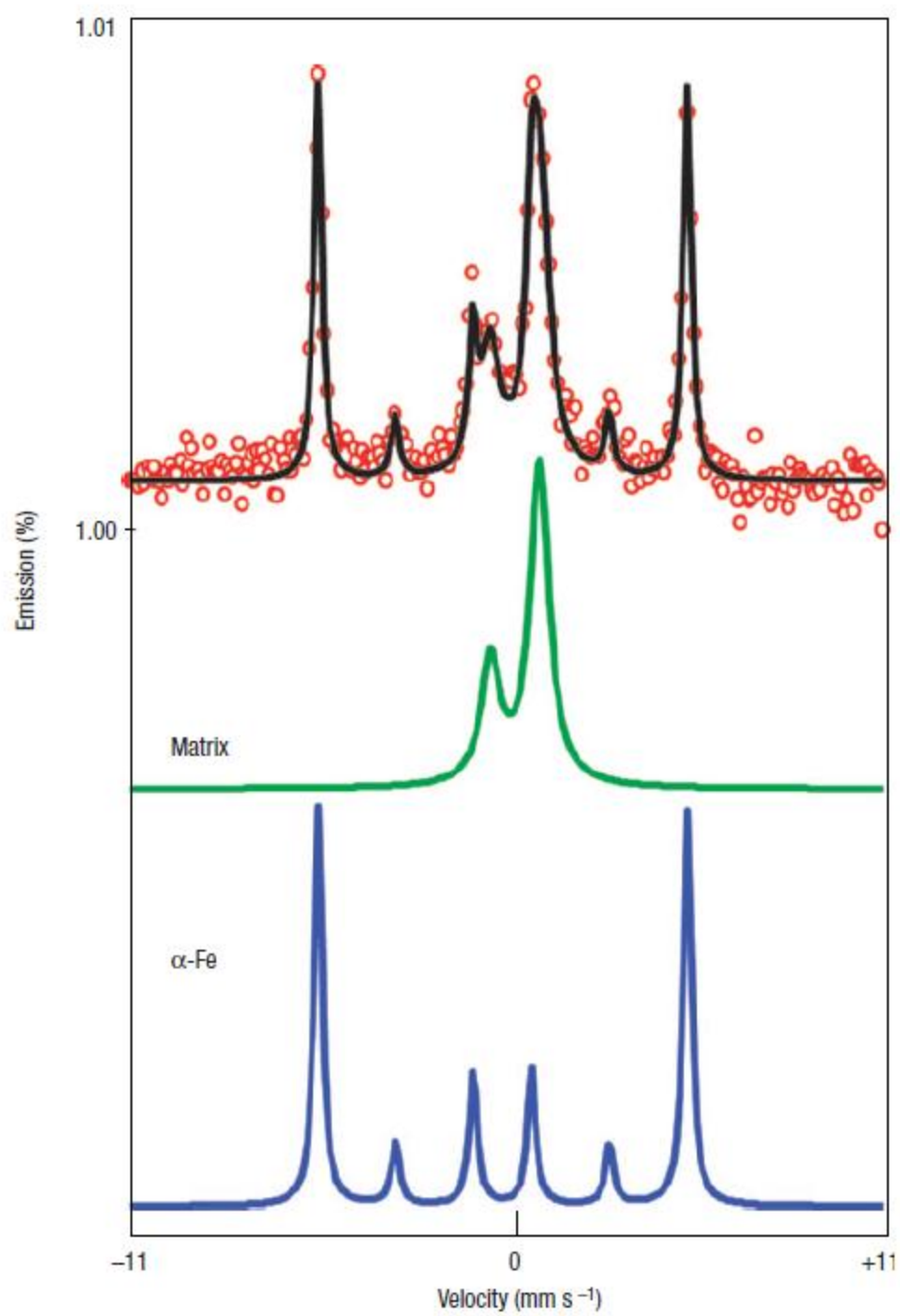
a

100 nm

b

220
200
400
220
Fe
110
200
110
LaSrFeO₄
000

c

Substrate
100 nm

Fig. 1

a 20 nm

b Fe nanowires 2 nm

Fig. 2

Fig. 3

a

M (e.m.u. cm⁻³) axis labeled from −2,000 to 2,000

ll to nanowire
⊥ to nanowires

Film deposited
in 200 mtorr O₂

H (kOe) axis labeled from −12 to 12

b

d = 20 nm

H_c (kOe) axis from 0 to 4

Aspect ratio (l/d) axis from 0 to 15

Inset: H_c (kOe) vs d (nm)

Fig. 4

Fig. 5